

Spatially resolved roughness exponent in polymer fracture

M. Thuy¹, A. Spyralis¹, M. Böhning¹, U. Niebergall¹ and R. Maass^{1,2,*}¹Federal Institute of Materials Research and Testing (BAM), Unter den Eichen 87, 12205 Berlin, Germany²Department of Materials Science and Engineering, University of Illinois at Urbana-Champaign, Urbana, Illinois 61801, USA

(Received 22 April 2022; accepted 29 August 2022; published 20 September 2022)

The fracture surface of slow and continuous crack propagation during environmental stress cracking of a semicrystalline polyethylene exhibits isotropic roughness exponents at the local scale but resolved across the macroscopic fracture surface a clear position dependence is found. The spatially resolved roughness exponent admits values in the range between 0.1 and 0.4, demonstrating nontrivial exponents in the small length-scale regime. Instead, they vary across the fracture surface according to the stress-state distribution, which suggests that the exponents are intimately linked to the locally dominating dissipation processes during craze cracking.

DOI: [10.1103/PhysRevMaterials.6.L090601](https://doi.org/10.1103/PhysRevMaterials.6.L090601)

The statistical quantification of fracture surfaces traces back to the pioneering work of Mandelbrot *et al.*, demonstrating fractal behavior [1]. Their insights established a link between self-affine scaling, i.e., objects remain upscaled or downscaled versions of each other across length scales within limiting bounds [2], and the complex surface morphologies known to appear after a crack has passed a solid. Since then fracture surfaces of a wide variety of materials, such as steels [3], aluminum alloys [4], sandstone [5], granite [6,7], wood [8], glasses [9], as well as polymers [10–13] have been shown to exhibit height-to-height fluctuations that can vary over several orders of magnitude and that obey scale-free statistics. This power-law behavior, delineated by the exponent as roughness exponent (or Hurst exponent), breaks down at a material specific correlation length ξ and is a manifestation of some microstructural length scale of the fracturing solid [14]. Indeed, ξ has frequently been reported to be the largest characteristic heterogeneity scale present in the microstructure, being for example the grain size in polycrystalline Ni [15], a dendritic length scale in Al [16,17], the size of opacifying secondary phases in glasses [18], or the spherulite size in semicrystalline polymers [19]. Yet, other studies reveal how ξ exceeds the fundamental microstructural length scale of the material, as for example for granite [6] or of sintered glass [20], which will also be the case for the here-investigated semicrystalline polyethylene.

Below ξ , the scaling exponent ζ describes the fractal behavior and is typically $\cong 0.8$ for surfaces originating from rapid unstable crack propagation [4,8,11,12,21,22]. Indeed, the (Hurst) exponent, H , quantified in this scaling regime, can directly be linked to the fractal dimension, D_f , of the investigated surfaces, yielding for a one-dimensional case $D_f = 2 - H$, where $1 < D_f \leq 2$ [23]. Here we will limit ourselves to investigating H . The numerically similar roughness exponent nurtured the view that ζ is universal since the scaling was independent of the material, fracture mode, and location on the fracture plane [24]. Even resolved spatially across the

entire fracture surface of a metal, the roughness exponents from unstable crack propagation exhibited universal behavior, being independent of the crack-propagation speed and the local stress state (plane strain or plane stress) [25].

Subsequently, more detailed studies were able to resolve crack propagation direction-dependent scaling exponents, defining ζ perpendicular and β parallel to the crack-propagation direction, and reporting a signature of anisotropic fracture dynamics [8,26,27]. Furthermore, ζ was reported to drop significantly to values $\cong 0.5$ [9,12,13] under controlled slow crack-propagation conditions, pointing towards length-scale dependent regimes and possible dominance of thermally-activated processes [28], which urged the need for more detailed investigations due to its relevance for both creep and fatigue stress-cracking failure [14]. This entails a focus on quasistatic crack-growth conditions, where the minimum surface-energy hypothesis may hold, since the fracture surface is expected to minimize the global fracture energy [29]. These developments shifted the focus away from a universal scaling behavior and underline the complex interplay between microstructure and driving factors (strain rate, stress state, etc.) that as of today are not fully understood. As such, this reminds very much of recent developments on intermittent and scale-free plasticity [30], where one first now begins to unravel the detailed dependencies of scaling exponents on microstructure and boundary conditions [31–33]. Indications of ζ admitting distinct length-scale dependent values ($\cong 0.5$ and $\cong 0.8$), anisotropy, and being sensitive to fracture kinetics therefore raise the question if local plastic dissipation and crack velocities may give rise to spatially heterogeneous roughness evolutions and scaling.

To shed more light onto this question, we consider here the specific case of polymers for which typical values of ζ close to 0.8 have been reported [12,13,21]. This is thus in agreement with other material types and therefore supports universal scaling in the large length-scale regime. For amorphous and semicrystalline polymers this can be rationalized by the homogeneous structure beyond a length scale of the macromolecular chain, or the scale given by distributed spherulites, as long as a processing-induced microstructural orientation is

*robert.maass@bam.de

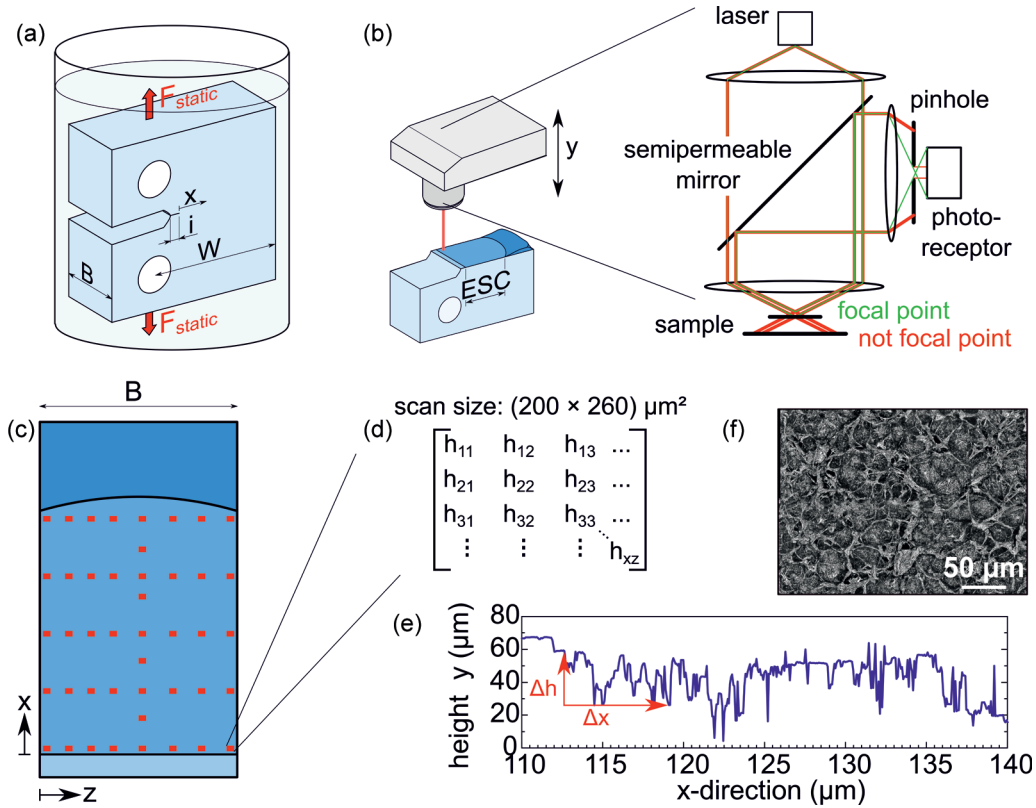


FIG. 1. Experimental procedure with (a) statically loaded CT specimen immersed in environmental medium 2 wt. % aq. Arkopal N100 at constant temperature of 40 °C. (b) Scanning of the ESC fracture surface performed by LSM with a pinhole in front of the photoreceptor to detect the reflected intensity for height identification. (c) Partition of local sections in the crack-propagation direction (x direction) and across the specimen thickness B (z direction). (d) Determined height matrix of one section. (e) Section of a height profile in crack-growth x direction for one column ($h_{11}, h_{21}, \dots, h_{x1}$). (f) Superimposed laser intensity and reflected light microscopic image of a section.

absent. These works have in common that they probe fracture surfaces of cryogenically cooled and subsequently impact-loaded specimens. In such a loading scenario fast cracking and therefore rapid crack propagation proceeds. Reducing the stress intensity factor in fatigue tests conducted below the fatigue threshold and thereby reducing the crack-propagation speed reveals indeed a reduced scaling exponent ($\zeta = 0.5$) [12]. This result underlines the qualitative sensitivity of ζ to the crack-propagation velocity, as also seen in some metals, and indicates that thermally-activated dissipative microplastic processes at and ahead of the crack tip become relevant [34]. Theoretically, this is captured as a regime in the vicinity of the depinning transition, where the crack front is just able to free itself from the microstructural pinning sites [28].

The observation of a crack-velocity dependent roughness exponent reported in the literature drives the hypothesis that its value is inherently linked to the microscopically and spatially varying crack dynamics. While the latter is almost impossible to track experimentally for opaque solids, it must naturally be linked to a position-dependent ζ -value, the value of which has the potential to shed light onto the local fracture and energy dissipation in slow crack growth (SCG) or environmental stress cracking (ESC) [14].

To this end, we track here the roughness exponent across the fracture surface of a prototypical semicrystalline high-density polyethylene (PE-HD). We find that the craze-crack mechanism of ESC yields a spatially varying roughness expo-

nent of values between 0.1 and 0.4 across the fracture surface. This scaling behavior persists irrespective of the analysis direction and ends at a spatially invariant correlation length that is a multiple of the largest identifiable microstructural length scale, which is the spherulite size. No direct dependence of ζ on the average crack-growth velocity can be found, but ζ evolves markedly different along the crack-growth direction for plane-strain and plane-stress conditions. This influence of local stress state drives different plastic dissipation processes at the crack front (craze crack with little plastic deformation vs volumetric plastic dissipation in the process zone), giving rise to the revealed spatial distribution of the roughness exponent. Thus, controlled ESC of a semicrystalline polymer suggests that local deformation mechanisms control the emerging roughness fluctuations on a fracture surface.

We investigate fracture surfaces obtained via static tensile loading ($F_{static} = 110\text{ N}$) of compact tension (CT) specimen stressed uniaxially in mode I [35]. During loading on an electronically controlled creep test system (Institut für Prüftechnik Gerätebau, IPT), the samples were immersed in a 40 °C tempered aqueous surfactant solution (2 wt. % aq. Arkopal N100), as schematically depicted in Fig. 1(a). The PE-HD specimens were milled from a hot-pressed and annealed 8-mm-thick sheet ($W = 35\text{ mm}$ and $B = 8\text{ mm}$) and a razor blade was used to introduce an initial notch ($i = 1\text{ mm}$) in the CT specimen, Fig. 1(a). Crack propagation up to final length of about 11 mm at static load consumed an experimental duration

of about 170 h. The subsequent transition towards ductile deformation is not taken into account. After ESC, the fracture surfaces were analyzed with a laser-scanning microscope (LSM, VK-X 100 of Keyence) using a 100× magnification lens. The LSM had a semiconductor laser operating at a wavelength of 658 nm and an output power of 0.95 mW. The confocal laser optics used a pinhole in front of the photoreceptor, which ensured that the highest light intensity at the focal point reaches the photoreceptor [Fig. 1(b)]. Using this LSM setup, the fracture surfaces were analyzed across different areas indicated in Fig. 1(c). The x axis in Fig. 1(c) begins at the initial notch position and describes the global crack-growth direction, whereas the perpendicular z axis globally describes the position along the crack front. Across each local area an array of about 3700×2800 positions was scanned to generate a height-value matrix [Figs. 1(d) and 1(e)] with a spatial resolution in the xz plane of 68.6 nm. The resolution along the optical axis (y axis) was determined to 5 nm. A typical fracture-surface image is shown in Fig. 1(f).

In order to investigate the topography of the fracture surface resulting from ESC, a 1D height-height correlation function along the crack-growth direction [x axis in Fig. 1(c)], Fig. 1(e)

$$\Delta h(\Delta x) = \langle (h(z, x + \Delta x) - h(z, x))^2 \rangle_{z,x}^{1/2} \quad (1)$$

and perpendicular to the crack-growth direction [z axis in Fig. 1(c)], along the crack front

$$\Delta h(\Delta z) = \langle (h(z + \Delta z, x) - h(z, x))^2 \rangle_{z,x}^{1/2} \quad (2)$$

is calculated for each local area indicated in Fig. 1(c). Figure 2 displays such data in a log-log representation, where arithmetic means of about 2800 line profiles in the crack-propagation direction (red color) and ~ 3700 line profiles perpendicular to the crack front (blue color) are summarized. That means, every height variance Δh for each step size of Δx or Δz results in the said 2800 or 3700 values, respectively, which are plotted in Fig. 2. This procedure was carried out for all examined local positions [Fig. 1(c)] with a measuring window of $(200 \times 260) \mu\text{m}^2$. The obtained trend of the used arithmetic mean is fitted linearly, where the fit between ~ 68 nm and $9 \mu\text{m}$ returns the smallest coefficient of determination that exceeds 0.99 in the present case. An uncertainty smaller than 0.01 was obtained for the power-law exponent. Error propagation of the experimental LSM values was not considered.

The subpanels (a) and (b) of Fig. 2 show exemplarily the data for four spatially resolved local areas at the specimen edge [Fig. 2(a)] and along the center line [Fig. 2(b)]. Clear power-law behavior for $\Delta h(\Delta z)$ or $\Delta h(\Delta x)$ smaller than approximately $9 \mu\text{m}$ is observed in all cases, which is also the case for the other studied local areas on the fracture surface.

The power-law scaling in Fig. 2 is a manifestation of the self-affine character of the fracture-surface roughness across more than two orders of magnitude until the correlation length of $\xi \approx 9 \mu\text{m}$ is reached. Beyond this point, the Δh scaling is lost and a regime is entered in which the fracture surface is typically referred to as a flat Euclidean object [12]. While earlier work has attributed ξ to a length scale representative of the microstructure [19] or a multiple of the microstructure

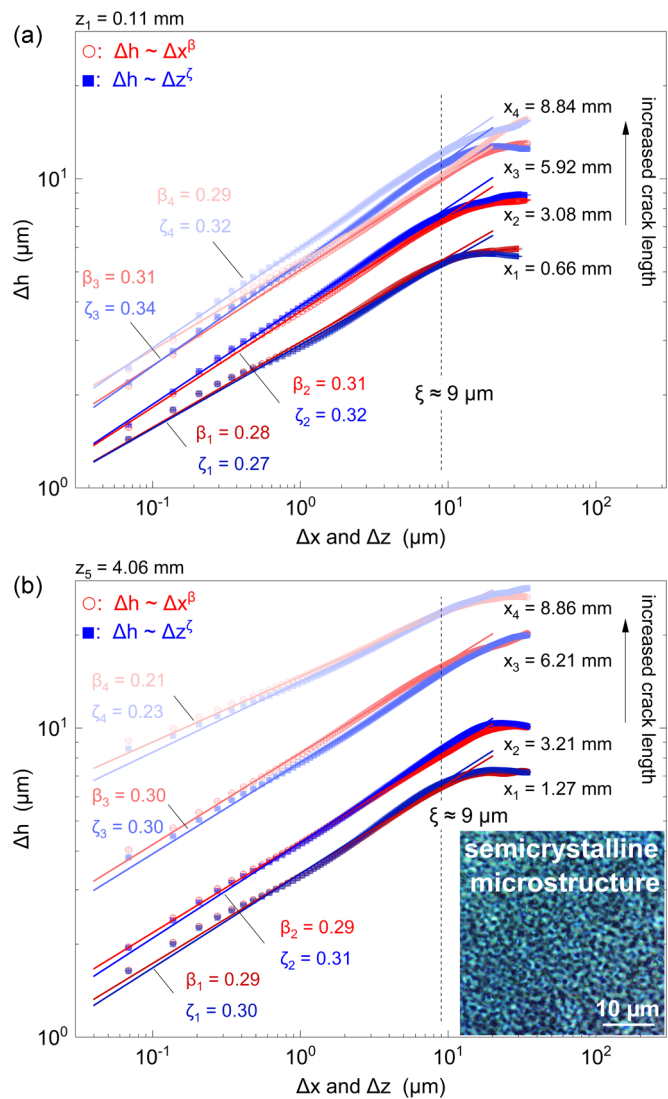


FIG. 2. Height-to-height fluctuations $\Delta h(\Delta x)$ parallel to the crack-propagation direction (\circ red color) and $\Delta h(\Delta z)$ perpendicular to it along the crack front (\square blue color) that obey scale-free statistics. Power-law behavior smaller than approximately $\xi \approx 9 \mu\text{m}$ is observed in all cases and exemplary for four local sections. Labels x_1 to x_4 denote the position on the fracture surface along the crack-growth direction with respect to the global coordinate system in Fig. 1(c) with (a) at the specimen edge ($z_1 = 0.11$ mm); (b) at the specimen center ($z_5 = 4.06$ mm). Inset in (b) reveals semicrystalline microstructure (polarized light micrograph) on a significantly smaller scale than ξ .

ture [26], its value is here about four times larger than the average spherulite size, as determined with polarized light microscopy from a 1- μm -thin cryomicrotome cut [inset in Fig. 2(b)]. This discrepancy is not surprising, considering that void forming during crazing initiates at the weakest inter-crystalline amorphous interfaces [36], of which the average distance will be larger than the spherulite size itself. This result holds also true when considering an $\sim 5\%$ decrease of the coefficient of determination for the linear fitting, which would yield a wide bound of 7.8 to 10.2 μm for ξ and thus would not change the present outcome. As such, these findings

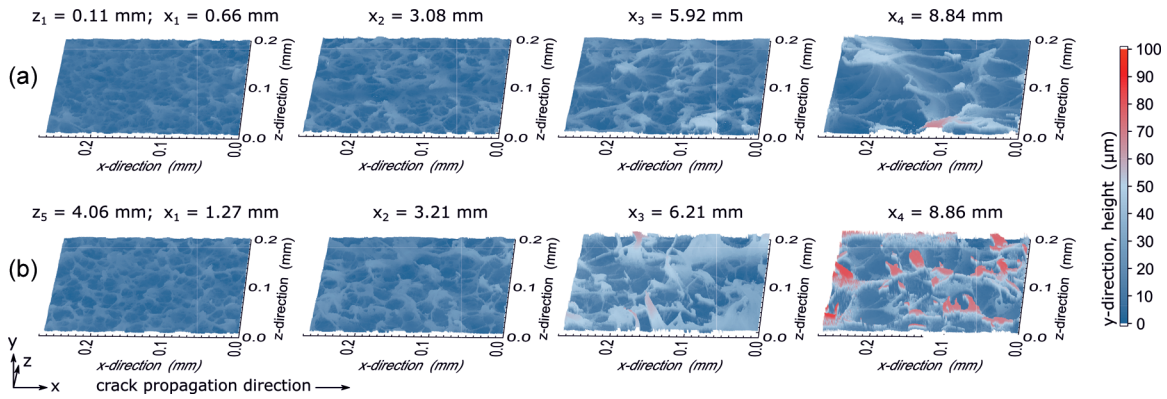


FIG. 3. Three-dimensional height profiles obtained using LSM for different investigated areas along the crack-growth direction near the specimen edge at $z_1 = 0.11$ mm and at the specimen center $z_5 = 4.06$ mm.

do not evidence any change of ξ with either the crack length [7,37] or the stress intensity factor [29], as seen in fast and uncontrolled crack propagation. This suggests that despite mechanistic changes during crazing at slow, quasistatic crack advance, no changes of the characteristic length-scale regime emerge.

Fitting the data in Fig. 2 with a power-law returns a direction-dependent scaling exponent in the crack-growth direction and along the crack-front direction, from now on defined as β and ζ , respectively. As can be seen, these exponents are varying from position to position, but at each locally evaluated area the exponents are, within the precision of the experiments, numerically identical (Fig. 2). The fact that β and ζ are the same for each individually evaluated area indicates locally isotropic fracture behavior [8], which is at odds with previous studies [12,13]. Since our semicrystalline polymer, apart from the crystalline and amorphous regions, has a homogeneous structure without process-induced orientation of the polymer chains, this result is at a first instance not surprising. Indeed, any subtle preferential crystallographic orientation is expected to affect the plastic processes ahead of the crack tip and the propagation path, thereby possibly giving rise to anisotropic roughness exponents. While the question of roughness isotropy or anisotropy remains an open question in the slow controlled-fracture regime, we note that earlier results for the fast-fracture regime imply that roughness anisotropy is not necessarily a consequence of material anisotropy. Indeed, the roughness along the direction perpendicular to the crack-propagation direction increases before it attains the self-similar regime [7]. This result should hold for microstructurally isotropic materials and would give rise to fracture anisotropy in an isotropic solid.

However, comparing the scaling exponent amongst the various positions across the entire fracture surface reveals a very different picture, where β and ζ vary substantially and in particular decrease with increasing distance along the crack-growth direction. This can be seen when comparing the differences between the pairs of height-to-height correlation datasets in Figs. 2(a) and 2(b). With increasing distance from the initial notch (x direction), the scaling exponents do not only decrease towards the fracture point, but there are further distinctly different evolutions of the exponents along different positions at constant z (crack-front direction). This

is exemplified for measurements along the specimen edge [$z_1 = 0.11$ mm, Fig. 2(a)], and the midline [$z_5 = 4.06$ mm, Fig. 2(b)]. The offsets between different datasets in Fig. 2 signify an increasing height-to-height variation with increasing crack length. These findings unambiguously demonstrate a spatially dependent roughness self-affinity, underlining the conclusion that invariance of β and ζ , as often suggested [4,8,11,12,21,22], is not a property of energy dissipation in adiabatic slow crack growth studied here. Figure 3 exemplifies the surface topographies along z_1 and z_5 as three-dimensional images from the obtained height profiles by LSM. Clear differences in the height fluctuations and surface morphology can be discerned for the regions closer to the edge (z_1) and those along the center line (z_5).

Given this position-dependent Hurst exponent, it is now instructive to map β and ζ across the entire fracture surface, which is depicted in Fig. 4, and for which the crack-propagation direction is along the abscissa. Crosses mark the positions at which local areas were investigated using Eqs. (1) and (2), and a linear interpolation between data points was done to produce the exponent surfaces. A point-to-point comparison between the β - and ζ maps shows good agreement between both quantities at each location, reinforcing the isotropic nature of local fracture.

The very similar spatial trends of both β and ζ reveal a center-symmetric pattern, where a slight increase from the crack-initiation site to the fracture point is seen at the outer sample edge ($z < 1$ mm and $z > 7$ mm) and a decrease emerges across the central fracture area. The latter is particularly apparent beyond a crack length of ~ 6 mm. The structural change on the fracture surface shown in Fig. 3 consequently entails the observed variation of the scaling exponent. Without having access to other locally varying properties beyond stress-states derived from classical linear elastic fracture mechanics, we use the calculated average crack velocity, dx/dt , for further analysis. Specifically, dx/dt has been determined from the monitored crack-opening displacement (COD), which itself was validated by a series of specimens where the COD was correlated with the average crack length after cryogenic fracture [35]. The resulting dx/dt quantity is shown in Fig. 5 together with the evolution of the Hurst exponents for $0 \text{ mm} < z \leq 4 \text{ mm}$ as a function of the crack-growth direction.

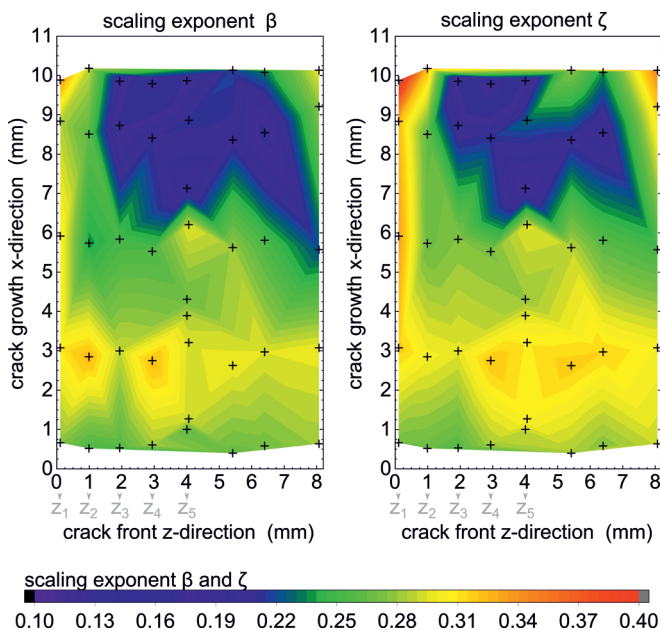


FIG. 4. Mapping of the measured spatially resolved scaling exponents (+) across the fracture surface including linear interpolation of the interspaces. Directional evaluation for β in crack-propagation x direction and ζ along the crack-front z direction yields numerically identical exponent evolution. Positions of z_1 to z_5 plotted for Fig. 5.

Clearly, both β and ζ increase initially with increasing crack-propagation velocity. Subsequently, a z -dependent evolution emerges, and a marked overall divergence between the scaling exponents sets in while the average crack velocity strongly increases. Specifically, β and ζ increase slightly from about $\beta \approx \zeta \approx 0.26$ close to the initial notch to about 0.30 to 0.33 ($x \approx 3$ mm), before decreasing continuously (starting

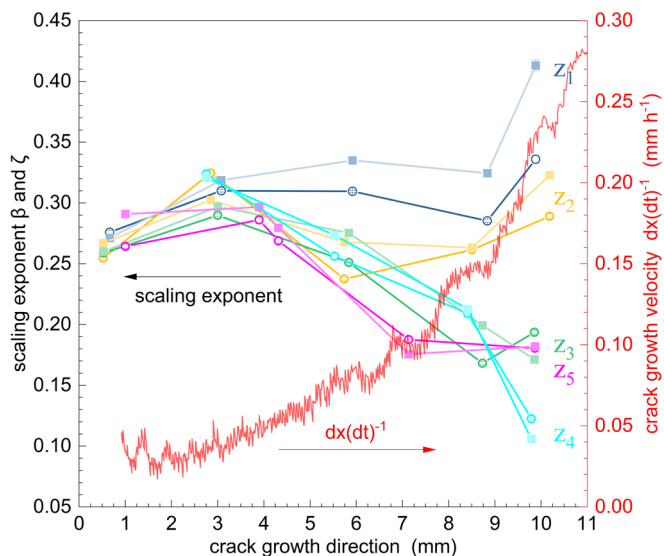


FIG. 5. Scaling exponent β (○) and ζ (□) as a function of crack length for the progression along the specimen edge (z_1) towards the progression in the specimen center (z_5) and calculated average crack speed across the specimen thickness.

at $x \approx 4$ mm) to 0.1 for the regions in the midline of the specimen. Contrary, β and ζ near the edge remain constant in the range of 0.27 to 0.32 or even exceed 0.40 for the outermost edge region. This evolution occurs axially symmetric relative to the specimen center line and suggests that the varying spatially roughness exponents is intimately connected to the crack speed.

Being related to the local stress state of the proceeding crack front, these results are in good agreement with a generally observed coarser fibril structure with increasing stress-intensity factor during stable crack propagation [38,39]. Such fibril coarsening originates from the viscoplastic response of the polymer during SCG or ESC, due to an increasing plastic zone size (damage halo [40]) ahead of the crack tip with continued crack propagation. While the crack accelerates, an increasing deformation volume participates in energy dissipation and available relaxation processes of the material become unable to counteract the far-field strain rate. This leads to larger craze-zone volumes, from which fibrils are formed via a meniscus instability mechanism [41] that subsequently are further elongated by surface drawing [42]. Such a general progression of the sizing structure with increasing local stress is a phenomenon that has been discussed in the context of other methods investigating ESC [39,43–45].

The fact that the edge regions exhibit a different roughness exponent evolution in comparison to the center region is attributed to the transition from a plane-strain to a plane-stress condition. Consequently, stress relaxation at the edge but in the thickness direction z is facilitated by transverse contraction. For sufficiently thick specimens, as is the case here, the transverse contraction in the center region is restricted by the neighboring surrounding material and a larger hydrostatic tensile stress arises. This triaxial and constraining stress state is known to significantly influence the crack-front propagation velocity. While from a statistical fracture perspective often modeled like a line moving through in a random microstructural environment based on a pinning-depinning transition [46], the continuum view provides a first good understanding of the divergent roughness exponent behavior seen in Figs. 4 and 5. In such a scenario, the average crack-front velocity develops from a straight line parallel to the initial crack front to a parabolic crack front due to larger front-propagation velocities in the specimen center [47,48]. This effect is known as crack tunneling and reflects a thickness-dependent crack-front velocity, where local near-crack-front distributions of the effective stress and deformation fields change significantly [49]. Alongside, with the transition from plane strain in the center of the specimen to plane-stress conditions at the side face, the critical stress intensity factor increases, which also manifests itself with decreasing specimen thickness [50,51]. These considerations provide a continuum-mechanics rationale for the divergent roughness exponents along the crack-propagation direction for $z_1 - z_2$ and $z_3 - z_5$ in Fig. 5.

At the microstructural level, the larger roughness exponents and therefore height-to-height variations for the near-side face region (plane stress) originates from shear lips where the amorphous intercrystalline regions accommodate shear displacements by glide between crystalline interfaces and fragmentation of the crystalline domains occurs [52]. In the central regions, where plane-stress conditions dominate, a

continued reduction of the height-to-height fluctuations with increasing crack propagation is due to dissipation processes involving a finer nucleation of microvoids and coalescence of cavities by disentanglement and overcoming intermolecular van der Waals forces, in which length scales of adjacent crazes and connecting molecules (tie molecules) become dominant [53]. These differences in plastic processes can be driven by the applied far-field deformation rate [54] but require orders of magnitude variation, meaning that the rise of the measured crack velocity in Fig. 5 is not a parameter controlling the roughness evolution. Instead, the stress state and related local crack-front velocity distribution controls the viscoplastic deformation mechanism that in turn determines the microscopically isotropic but at macroscopically position-dependent roughness exponent.

In summary, environmental stress cracking in a semicrystalline polymer reveals roughness exponents derived from the fracture surface that overall are in agreement with the numerically smaller values than observed at unstable fast cracking. In addition, we can show how the exponents indicate isotropic

fracture at the local scale, but that there are systematic changes across the fracture surface, with exponents ranging from 0.10 to 0.41. This spatially resolved fracture exponent follows a pattern much in agreement with the stress-state transition from plane-stress to plane-strain conditions that are known to determine the local viscoplastic dissipation at sufficiently slow crack growth. We anticipate that this would also be the case for metals fracture, or other solids that deform at sufficiently low timescales, for ample plastic dissipation via thermally-activated processes, suggesting that roughness exponents are intimately linked to the local dominating deformation mechanism.

M.T. is grateful for financial support of AiF within the program for sponsorship by Industrial Joint Research (IGF) of the German Federal Ministry of Economic Affairs and Climate Action, IGF Grant No. 20673N. The authors thank I. Alig and H. Oehler from the Fraunhofer Institute for Structural Durability and System Reliability LBF, as well as A. Kranzmann from the BAM for valuable and fruitful discussions.

-
- [1] B. B. Mandelbrot, D. E. Passoja, and A. J. Paullay, *Nature (London)* **308**, 721 (1984).
- [2] K. Foroutan-pour, P. Dutilleul, and D. L. Smith, *Appl. Math. Comput.* **105**, 195 (1999).
- [3] A. S. Balankin, *Eng. Fract. Mech.* **57**, 135 (1997).
- [4] M. Hinojosa, E. I. Morales, and N. Mohamed, in *Advanced Structural Materials III*, edited by H. B. Ramirez, J. G. Cabanas-Moreno, H. A. Calderon-Benavides, K. Ishizaki, and A. Salinas-Rodriguez (Trans Tech Publications Ltd, Durnten-Zurich, 2007), pp. 91.
- [5] H. P. Xie and J. A. Wang, *Int. J. Solids Struct.* **36**, 3073 (1999).
- [6] J. Schmittbuhl, F. Schmitt, and C. Scholz, *J. Geophys. Res.-Solid Earth* **100**, 5953 (1995).
- [7] J. Schmittbuhl, S. Roux, and Y. Berthaud, *Europhys. Lett.* **28**, 585 (1994).
- [8] L. Ponson, D. Bonamy, H. Auradou, G. Mouro, S. Morel, E. Bouchaud, C. Guillot, and J. P. Hulin, *Int. J. Fract.* **140**, 27 (2006).
- [9] M. Hinojosa, E. Reyes-Melo, C. Guerra, V. Gonzalez, and U. Ortiz, *Int. J. Fract.* **151**, 81 (2008).
- [10] K. Arakawa and K. Takahashi, *Int. J. Fract.* **48**, 103 (1991).
- [11] C. Guerrero, E. Reyes, and V. Gonzalez, *Polymer* **43**, 6683 (2002).
- [12] M. Hinojosa, V. Gonzalez, J. Sanchez, and U. Ortiz, *Polymer* **45**, 4829 (2004).
- [13] F. Lapique, P. Meakin, J. Feder, and T. Jossang, *J. Appl. Polym. Sci.* **86**, 973 (2002).
- [14] M. J. Alava, P. Nukalaz, and S. Zapperi, *Adv. Phys.* **55**, 349 (2006).
- [15] M. Hinojosa, E. Bouchaud, and B. Nghiem, in *Symposium on Fracture and Ductile vs Brittle Behavior-Theory, Modelling and Experiment, at the 1998 Fall Meeting* (Materials Research Society, Boston, 1998), pp. 203.
- [16] M. Hinojosa, J. Aldaco, U. Ortiz, and V. González, *Alum. Trans.* **3**, 53 (2000).
- [17] M. Hinojosa and J. Aldaco, *J. Mater. Res.* **17**, 1276 (2002).
- [18] E. Reyes, C. Guerrero, and M. Hinojosa, *Emergent Nature*, **385** (2002).
- [19] M. Hinojosa, J. Aldaco, U. Ortiz, and J. A. Gonzalez, in *European Conference on Advances in Mechanical Behaviour, Plasticity and Damage (EUROMAT 2000)* (Elsevier Science Bv, Tours, France, 2000), pp. 1469.
- [20] L. Ponson, H. Auradou, P. Vie, and J. P. Hulin, *Phys. Rev. Lett.* **97**, 125501 (2006).
- [21] E. Reyes, C. Guerrero, V. Gonzalez, and M. Hinojosa, in *Multiscale Phenomena in Materials-Experiments and Modeling*, edited by I. M. Robertson, D. H. Lassila, B. Devincere, and R. Phillips, (Materials Research Soc., Warrendale, 2000), pp. 357.
- [22] J. Schmittbuhl, S. Gentier, and S. Roux, *Geophys. Res. Lett.* **20**, 639 (1993).
- [23] M. Q. Jiang, J. X. Meng, J. B. Gao, X. L. Wang, T. Rouxel, V. Keryvin, Z. Ling, and L. H. Dai, *Intermetallics* **18**, 2468 (2010).
- [24] E. Bouchaud, G. Lapasset, and J. Planès, *Europhys. Lett.* **13**, 73 (1990).
- [25] P. Kotowski, *Int. J. Fract.* **141**, 269 (2006).
- [26] L. Ponson, D. Bonamy, and E. Bouchaud, *Phys. Rev. Lett.* **96**, 035506 4,(2006).
- [27] D. Bonamy, L. Ponson, S. Prades, E. Bouchaud, and C. Guillot, *Phys. Rev. Lett.* **97**, 135504 (2006).
- [28] P. Daguier, B. Nghiem, E. Bouchaud, and F. Creuzet, *Phys. Rev. Lett.* **78**, 1062 (1997).
- [29] E. Bouchaud and J. P. Bouchaud, *Phys. Rev. B* **50**, 17752 (1994).
- [30] J. P. Sethna, M. K. Bierbaum, K. A. Dahmen, C. P. Goodrich, J. R. Greer, L. X. Hayden, J. P. Kent-Dobias, E. D. Lee, D. B. Liarte, X. Y. Ni, K. N. Quinn, A. Raju, D. Z. Rocklin, A. Shekhawat, and S. Zapperi, in *Annual Review of Materials Research*, edited by D. R., Clarke, Vol. 47 (Annual Reviews, Palo Alto, 2017), pp. 217.
- [31] G. Sparks and R. Maass, *Phys. Rev. Mater.* **2**, 120601(R) (2018).
- [32] G. Sparks and R. Maass, *Eur. Phys. J. B* **92**, 15 11,(2019).
- [33] G. Sparks and R. Maass, *Acta Mater.* **152**, 86 (2018).

- [34] R. Maass and P. M. Derlet, *Acta Mater.* **143**, 338 (2018).
- [35] M. Thuy, M. Pedragosa-Rincón, U. Niebergall, H. Oehler, I. Alig, and M. Böhning, *Polymers* **14**, 2415 (2022).
- [36] A. Y. Yarysheva, E. G. Rukhlya, L. M. Yarysheva, D. V. Bagrov, A. L. Volynskii, and N. F. Bakeev, *Eur. Polym. J.* **66**, 458 (2015).
- [37] E. Bouchaud and S. Navéos, *J. Phys. I France* **5**, 547 (1995).
- [38] S. Bandyopadhyay and H. R. Brown, *Polymer* **22**, 245 (1981).
- [39] S. Bandyopadhyay and H. R. Brown, *J. Polym. Sci. Pt. B: Polym. Phys.* **19**, 749 (1981).
- [40] S. K. Bhattacharya and N. Brown, *J. Mater. Sci.* **20**, 2767 (1985).
- [41] E. J. Kramer, *Crazing in Polymers*, edited by H. H. Kausch (Springer Berlin Heidelberg, 1983), pp. 1–56.
- [42] Y. J. Tang, Z. Y. Jiang, H. F. Enderle, D. Lilge, S. V. Roth, R. Gehrke, J. Rieger, L. J. An, and Y. F. Men, *Chin. J. Polym. Sci.* **28**, 165 (2010).
- [43] R. Deblieck, B. Gerets, M. Boerakker, H. Caelers, A. Wilbers, and T. Boonen, *Polymer* **176**, 264 (2019).
- [44] M. Thuy, U. Niebergall, H. Oehler, I. Alig, and M. Böhning, *Polymer* **228**, 123853 (2021).
- [45] G. Pinter and R. W. Lang, *J. Appl. Polym. Sci.* **90**, 3191 (2003).
- [46] E. Bouchaud, *J. Phys.: Condens. Matter* **9**, 4319 (1997).
- [47] J. J. Strebel and A. Moet, *J. Mater. Sci.* **26**, 5671 (1991).
- [48] J. J. Strebel and A. Moet, *Polym. Eng. Sci.* **33**, 217 (1993).
- [49] W. M. Lan, X. M. Deng, and M. A. Sutton, *Eng. Fract. Mech.* **77**, 2800 (2010).
- [50] H. Liu, X. G. Yang, S. L. Li, D. Q. Shi, and H. Y. Qi, *Int. J. Mech. Sci.* **178**, 105625 (2020).
- [51] J. Garcia-Manrique, D. Camas, P. Lopez-Crespo, and A. Gonzalez-Herrera, *Int. J. Fatigue* **46**, 58 (2013).
- [52] M. Contino, L. Andena, and M. Rink, *Eng. Fract. Mech.* **241**, 107422 (2021).
- [53] R. A. C. Deblieck, D. J. M. van Beek, K. Remerie, and I. M. Ward, *Polymer* **52**, 2979 (2011).
- [54] R. Gensler, C. J. G. Plummer, C. Grein, and H. H. Kausch, *Polymer* **41**, 3809 (2000).